heritage

MDPI

Article

Development of a Hyperspectral Imaging Protocol for Painting Applications at the University of Seville

Giovanna Vasco [1,*], Hélène Aureli [2], Isabel Fernández-Lizaranzu [3], Javier Moreno-Soto [2], Anabelle Križnar [4], Rubén Parrilla-Giraldez [3], Emilio Gómez-González [3] and Miguel Angel Respaldiza Galisteo [2]

1 Bibliothèque nationale de France (BnF), Quai François Mauriac, 75013 Paris, France
2 Centro Nacional de Aceleradores (CNA), C. Tomás Alva Edison, 7, 41092 Seville, Spain; haureli@us.es (H.A.); jmoreno53@us.es (J.M.-S.); respaldiza@us.es (M.A.R.G.)
3 Group of Interdisciplinary Physics (GFI), School of Engineering (ETSI), Avenida Camino de los Descubrimientos, 41092 Seville, Spain; ifernandez14@us.es (I.F.-L.); rparrilla@us.es (R.P.-G.); egomez@us.es (E.G.-G.)
4 Department of Sculpture and Art History, Faculty of Fine Arts, University of Seville, C/Laraña 3, 41003 Seville, Spain; akriznar@us.es
* Correspondence: giovanna.vasco@bnf.fr

Abstract: In the last decade, the hyperspectral imaging (HSI) method allowed performing non-invasive analysis in the field of cultural heritage. However, a considerable limitation was given by redundant and time-consuming features, with the necessary application of statistical algorithms and image-processing tools to extract relevant information. In this study, the Centro Nacional de Aceleradores (CNA) and the Group of Interdisciplinary Physics (GFI) of the School of Engineering (ETSI) of the University of Seville tested the application of three different hyperspectral cameras in the visible and near-infrared (VNIR) and short-wave infrared (SWIR) range for the investigation of an ancient painting. A reference-based procedure was realised to build a starting personal library and to evaluate the best working conditions for non-invasive and non-destructive characterisation with data treatment using the commercially available software Evince® and Specim IQ® to apply, respectively, the Principal Component Analysis (PCA) model functions and the classification method. The evaluation of the protocol was tested by acquiring complementary information by X-ray fluorescence (XRF), Ultraviolet Luminescence (UVL) imaging, and Infrared Reflectography (IRR). This exploration established a simplified protocol to analyse the large collection of paintings of the Archbishop's Palace and the Cathedral of Seville.

Keywords: VNIR; SWIR; XRF; protocol validation; hyperspectral imaging (HSI) method; PCA; paintings

Citation: Vasco, G.; Aureli, H.; Fernández-Lizaranzu, I.; Moreno-Soto, J.; Križnar, A.; Parrilla-Giraldez, R.; Gómez-González, E.; Respaldiza Galisteo, M.A. Development of a Hyperspectral Imaging Protocol for Painting Applications at the University of Seville. *Heritage* **2024**, *7*, 5986–6007. https://doi.org/10.3390/heritage7110281

Academic Editor: Georgios P. Mastrotheodoros

Received: 10 August 2024
Revised: 4 October 2024
Accepted: 10 October 2024
Published: 23 October 2024

1. Introduction

In recent years, hyperspectral imaging (HSI) techniques have gained significant recognition for their ability to perform non-invasive and non-destructive analyses as a rapid initial screening method without the use of harmful radiation [1–7]. Advances in solid-state sensor technology have facilitated the application of this analytical method in remote sensing across a wide range of fields, including pharmaceuticals, environmental science, industrial quality control, and the agri-food sector [8–15]. The narrow and numerous bandwidths of HSI provide greater accuracy than multispectral imaging systems (MSI) in mapping material distribution, achieved by digitally extrapolating spectroscopic information from false colours [16–18]. Furthermore, the hyperspectral cube of images generated during the scan at different wavelengths enables the remote extraction of reflectance spectra from each pixel at any time [9,19].

In the field of cultural heritage, hyperspectral cameras are used to reveal the presence of underdrawings and pentimenti, identify pigments, faded paints, inks, and traces of lost materials that are not visible to the naked eye, as well as to detect potential remnants

of previous conservation materials and treatments [19–29]. Furthermore, HSI offers several advantages: it collects spectral data from entire scanned areas, thereby eliminating the risk of missing information that can occur with point analysis methods [30]; it uses portable devices for in situ applications [31–33]; it produces high-quality images with colour corrections for artwork documentation [34,35]; and it records *craquelure* to monitor the conservation status of the painted layer [36–38].

Nevertheless, light sources and exposure times must be used with caution due to the presence of photosensitive materials [39,40]. Additionally, results can be influenced by various factors, including scan speed, non-homogeneous illumination, uncorrected calibration, differing instrumental sensitivity, and thermal exposure. Although effective guidelines have been established to address potential drawbacks related to proper illumination and lens adjustments for improved acquisitions, certain aspects remain challenging.

Indeed, pigment recognition has been suggested through the use of commercially available colour reference targets by comparing colour rendering at different wavelengths [18,41]. Furthermore, the reliability, handling, and processing of the data depend on various factors, including instrumental specifications, operating conditions, system characteristics, management software, and file formats [1,19,41]. Therefore, it is essential to develop standardised and simplified procedures for systematic use in cultural heritage investigations, particularly for painting applications. Although the extraction of spectral information from mixed materials is theoretically possible using the Kubelka-Munk theory, the procedure remains challenging, and colour references are primarily available for pure pigments [42–45]. Nevertheless, these references are difficult to apply when pigments are combined with binders, especially within multi-layer pictorial materials. Additionally, data storage capacity, advanced processing requirements, and the extraction of extensive spectral data can be both redundant and time-consuming. Consequently, the application of statistical algorithms and image processing tools is a crucial step in minimising data size and enhancing the extraction of relevant information [25,46]. Among the various classification methods employed to reduce dimensionality and improve class separability, principal component analysis (PCA) has been used in conservation science to eliminate redundant data [47–50]. Nevertheless, several laboratories have developed proprietary tools using non-commercial software that incorporates artificial intelligence for pigment classification [51]. Thus, conservation laboratories continue to face difficulties in the consistent application of these scientific tools.

The collaboration between the Centro Nacional de Aceleradores (CNA) and the Group of Interdisciplinary Physics (GFI) enabled the exploration of various hyperspectral cameras equipped with push-broom spectrometers for the investigation of ancient paintings. The primary aim of this study was to extend the non-invasive and non-destructive pigment characterisation, thereby providing consistent support to the Archbishop's Palace Conservation Laboratory and the Cathedral of Seville [52]. A specific case study was conducted on a 17th-century painting titled *Virgen con niño*, belonging to the collection at the Archbishop's Palace. This study employed a portable and compact hyperspectral camera operating within the visible and near-infrared (VNIR) range, in addition to two hyperspectral cameras mounted on a motorised stage working, respectively, the visible and near-infrared (VNIR) and the short-wave infrared (SWIR) ranges. The integration of these three cameras allowed the evaluation of a simple standard-based protocol to gain reproducible and comparable data for applications on paintings. Measurement and data processing were conducted using a well-established image processing software (Evince®), which provided tools for extracting and refining information from the hyperspectral cube, thereby enabling a straightforward survey applicable to polychrome surfaces. Furthermore, a rapid classification method for paintings was developed for the handheld hyperspectral camera using software provided by Specim IQ®. The protocol was validated by collecting complementary information from the case study through the application of X-ray fluorescence (XRF), Ultraviolet Luminescence (UVL) imaging, and Infrared Reflectography (IRR). As a result, a simplified protocol was provided to the Conservation Laboratory, thereby

enabling conservators to extend the application of hyperspectral cameras for routine use prior to painting restoration.

2. Materials and Methods

For a comprehensive investigation of painting artworks, two push-broom hyperspectral cameras (VNIR and SWIR) operating with the use of a motorised structure housed within the laboratories of the Group of Interdisciplinary Physics were tested [53] to cover a portion of light, ranging from the visible (406.62–996.46 nm) to the short-wave infrared (879–1688 nm). The VNIR camera was specifically applied for identifying and mapping pigments, while the SWIR camera facilitated the documentation of potential underdrawings. Additionally, given the significant artistic heritage displayed in the Cathedral of Seville, a portable handheld VNIR camera (400–1000 nm) was used to establish optimal working conditions for in situ applications.

To validate the method (Figure 1), an initial test was conducted on wooden panels with known painted layers (refer to Section 2.1.1). This test aimed to establish a small reference database comprising the most common pigments encountered by conservators and heritage scientists within the Archbishop's Palace collection. As shown by Figure 1, the facilitated protocol was intended as a reiterative protocol, expanding the application by adding references in dependence on the pigments of interest. The development of these reference-painted tablets was planned to assess the different sensitivity in depth between the applications of the VNIR and SWIR cameras when analysing multi-layered materials with different binders. Additionally, it was considered that the reflectance spectra might be influenced by the optical opacity or transparency of the painted layers.

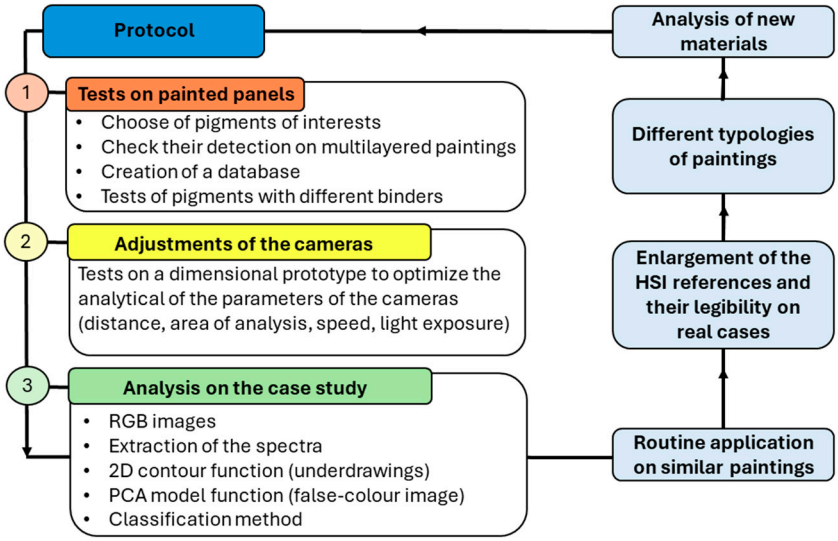

Figure 1. Steps for the validation of the HSI method on paintings.

Furthermore, it was possible to identify both advantages and potential drawbacks within the adjustment of working parameters and the establishment of data management protocols for the extraction of spectral and spatial features. Subsequently, both push-broom and portable hyperspectral cameras were used to investigate a 17th-century oil painting (70 × 50 cm) titled *Virgen con niño*, which was preliminary observed using non-invasive and non-destructive methods with the portable equipment. Indeed, the application of additional methods was necessary to verify the results from the hyperspectral cameras, double-checking the pigment detection and the presence/absence of the underdrawing and retouches. Specifically, complementary information regarding the pigment palette was acquired through X-ray Fluorescence (XRF), while retouched areas and the potential presence of underdrawings or *pentimenti* were identified using ultraviolet luminescence (UVL) and infrared reflectography (IRR), respectively.

2.1. Application on Pigments

2.1.1. Reference Painted Panels

A total of sixteen painted panels (100 cm^2) were realised to verify the influence on the spectral information of the presence of several pigments, applied in a combination of several layers. The wooden panels were prepared by applying a layer of rabbit glue to the surface, followed by a ground layer made of stucco made from rabbit glue and calcium sulphate. The thickness of each layer, measuring 1 mm, was monitored using a micrometre. Subsequently, each panel was divided into four squares, where different graphite drawings were created at the centre of a circle. Following this, the panels were coated with a priming layer, approximately 250 µm in thickness, which contained either white lead or haematite, mixed with linseed oil and cobalt siccative (Table 1). The panels were designated as W (white) or R (red) based on the use of white lead or haematite for the priming layer.

Table 1. List of the different layers of pigments applied on eleven painted panels.

Name	Priming Layer (Square 1)	First Layer (Square 2)	Second Layer (Square 3)	Third Layer (Square 4)
W1	White lead	White	Malachite	Yellow ochre
W2	White lead	Lead-tin yellow	Haematite	Azurite
W3	White lead	White lead	Lead-tin yellow	Vermilion
W4	White lead	Haematite	Azurite	White lead
W5	White lead	Haematite	Vermilion	Lead-tin yellow
W6	White lead	Lead-tin yellow	Haematite	Azurite
W7	White lead	White lead	Lead tin yellow	Vermilion
W8	White lead	Haematite	Vermilion	Lead-tin yellow
R1	Haematite	White lead	Lead-tin yellow	Vermilion
R2	Haematite	Haematite	Azurite	White lead
R3	Haematite	Haematite	Vermilion	Lead-tin yellow

The following pigments, arranged differently on the panels, commonly used in 16th- and 17th-century paintings, were used to create a reference library:

- white lead ($2PbCO_3 \cdot Pb(OH)_2$)
- lead-tin yellow (Pb_2SnO_4)
- verdigris ($Cu(CH_3CO_2)_2 \cdot (H_2O)$)
- malachite ($Cu_2(CO_3)(OH)_2$)
- yellow ochre ($Fe^{3+}O(OH)$)
- vermilion (HgS)
- haematite (Fe_2O_3)
- carmine red ($C_{22}H_{20}O_{13}$)
- ultramarine ($Na_7Al_6Si_6O_{24}S_3$)
- azurite ($Cu_3(CO_3)_2(OH)_2$)

Eleven of the reference panels (Figure 2) were prepared, leaving the priming layer in the top-left square and painting the remaining area with the first painted layer. The third and fourth squares were then painted with the second painted layer. Finally, the third painted layer was applied in the fourth square only. The various arrangements of the pigments are listed in Table 1.

Moreover, two further panels (W9, R4) were painted, realising a single layer of four squares consisting of vermilion, yellow ochre, malachite, and azurite. Three additional panels (TE1, LO1, AG1) were painted using different binders (tempera based on egg, linseed oil, and animal glue). In these three panels, a single layer of malachite, carmine,

ultramarine, and verdigris has been applied to each of the four squares. The preparation of these last five panels is summarised in Table 2.

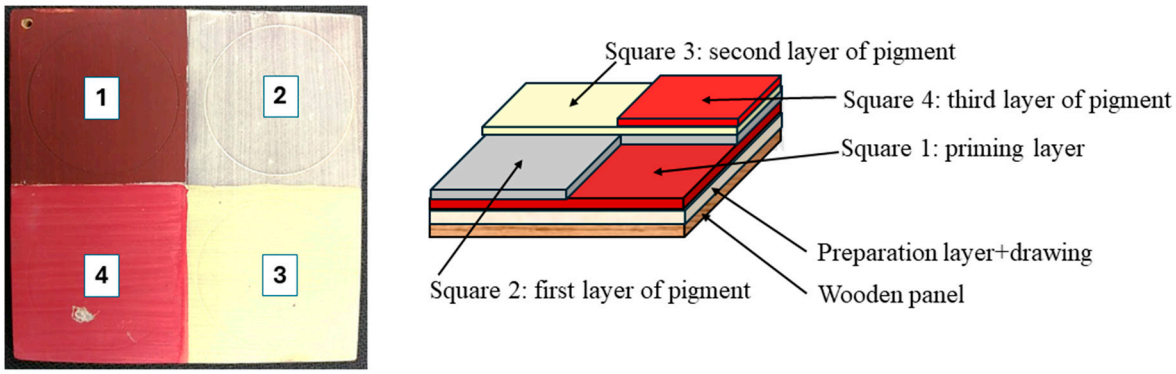

Figure 2. Structure of multilayered reference panels to test the possible detection of the underdrawings and the spectra of the pigments in dependence on the opacity of the pigments and their different arrangements.

Table 2. Painted panels with applied pigments in different areas of the priming layer.

Name	Priming Layer	Pigment 1 (Square 1)	Pigment 2 (Square 2)	Pigment 3 (Square 3)	Pigment 4 (Square 4)
W9	White lead	Vermilion	Yellow ochre	Malachite	Azurite
R4	Haematite	Malachite	Azurite	Vermilion	Yellow ochre
TE1	Binder: tempera based on egg				
	White lead	Malachite	Carmine	Ultramarine	Verdigris
LO1	Binder: linseed oil				
	White lead	Malachite	Carmine	Ultramarine	Verdigris
AG1	Binder: animal glue				
	White lead	Malachite	Carmine	Ultramarine	Verdigris

2.1.2. Selected Areas from a 17th-Century Oil Painting

An exploratory investigation was conducted using a real case study to apply the hyperspectral imaging method and data analysis on a 17th-century oil painting, *Virgen con niño*, by an anonymous artist, today stored in the Archbishop's Palace in Seville (Figure 3A).

To prevent hazards from handling and potential damage induced by prolonged exposure to the light sources of the hyperspectral cameras during the experimental parameter setting, a piece of cardboard was cut to the same size as the painting and its gilded wooden frame. An approximate drawing, similar to the dimensions of the painting, was made by dividing the area into squares of ~5 × 5 cm^2 in order to find the best analysis conditions at different distances (Figure 3B,C). In this way it was possible to check the radiation distribution and adjust the light sources, the focus, and the parameters relating to the movement and speed of the hyperspectral cameras, thus limiting any unnecessary risk to the work of art. To preserve spatial references, the real oil painting was subdivided into squares (~5 × 5 cm^2) using a wire grid (Figure 3D).

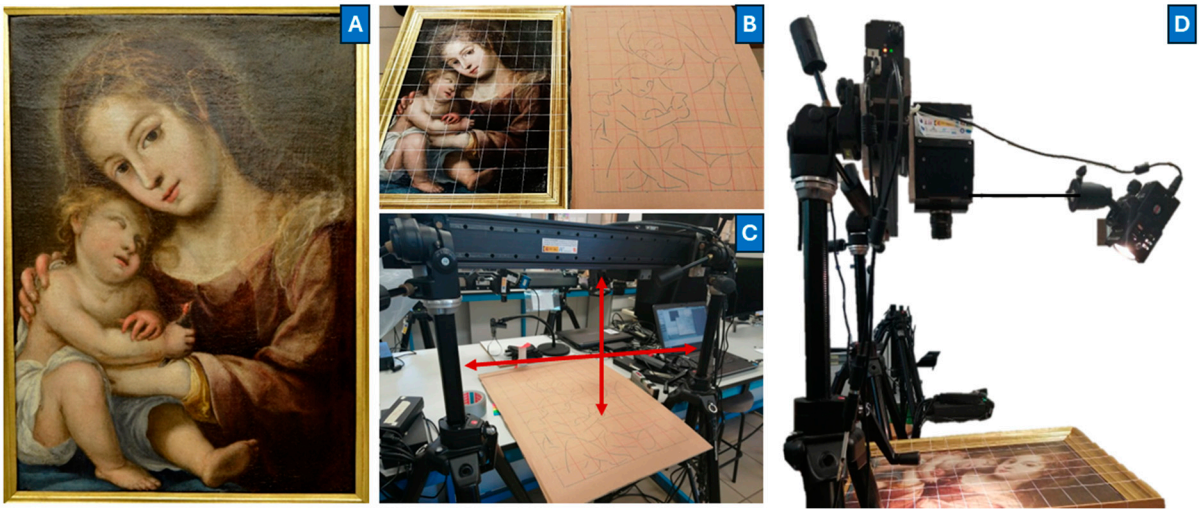

Figure 3. Painted objects analysed by using the hyperspectral imaging method: the 17th-century oil painting *Virgen con niño* (**A**) from the Conservation Laboratory of the Archbishop's Palace and the Cathedral of Seville, and the cardboard replica (**B**) for the evaluation of the light distribution and the camera parameters (**C**) before the analysis on the real painting (**D**) to avoid hazards.

2.2. Hyperspectral Cameras

The A-Series VNIR hyperspectral camera (Headwall®, Bolton, MA, USA), equipped with a Si CCD sensor and a 35 mm LM35HC lens (KOWA®, Saitama, Japan), was used to obtain the reflectance spectra of the analysed areas both on the reference painted panels and the oil painting. The spectral wavelengths ranged from 406.62 to 996.46 nm (covering 810 bands) with a nominal spectral resolution of 0.74 nm.

A short-wave infrared hyperspectral camera (SWIR) (Goldeye® G-008 TEC1, Allied Vision, Germany) with an InGaAs sensor was employed to investigate the reflectance spectra of the analysed areas, specifically targeting the presence of underdrawings, with a resolution of 320 (H) × 256 (V) × 30 µm. The spectral wavelengths for this camera ranged from 879 to 1688 nm.

These two cameras were positioned on a motorised linear translation stage (A-LST0750-C Zaber®, Zaber, Vancouver, BC, Canada), and an ASD Illuminator halogen light source (Malvern Panalytical®, Worcestershire, UK) was placed above the sample plane at a 45-degree angle with the vertical line. The light source was installed alongside the camera to move simultaneously.

The compact handheld VNIR portable snapshot camera (Specim IQ® Specim, Spectral Imaging Ltd, Finland) operates in the range of 400–1000 nm, with a resolution of 7 nm, 3.5 nm spectral sampling, and 204 spectral bands. It features a CMOS sensor, and the image resolution is 512 × 512 pixels. The camera was mounted on a tripod in front of a portable darkroom to prevent interference from natural light. Two ASD illuminators were symmetrically arranged at 45° with respect to the normal plane of the painting to ensure homogenous illumination of the sample area.

Different tests concerning distance and focus parameters were performed, as using long working distances to capture images in large areas results in a significant loss of resolution. On the other hand, high magnification with short focal distance on small areas to achieve high-resolution images generates large files (>3 GB) that are difficult to process and store. To strike a balance, the hyperspectral cameras were set with the parameters shown in Table 3, capturing tiles of 10 × 10 cm^2. These images acquired with the cameras on the motorised linear translation stage were stacked together using the open-source ImageJ software (version 1.54k). Regarding the compact handheld camera, the pictures were taken at different distances, ranging from a single image of the entire oil painting to select areas measuring 30 × 30 cm^2.

Table 3. Working parameters of the hyperspectral cameras.

Hyperspectral Cameras	Push-Broom		Snapshot
	VNIR	**SWIR**	**VNIR**
Focus distance	48 cm	47 cm	31 cm
Exposure	3000 a.u.	10,000 µs	14 ms
Speed	3.38 sec per tile	4.7 mm/s	-
Frame period	25,000 a.u.	10,000 Hz	1′23″
Light position	45°	45°	45°
Irradiance	0.1×10^{-3} W/m^2	1.4×10^{-3} W/m^2	0.8×10^{-3} W/m^2

During the analyses, the environmental parameters were T = 25 °C and RH = 44%.

For all cameras working on the motorised stage, calibration was performed by obtaining a white correction (99% reflectance) using a uniform Teflon specimen as the spectral standard reference. A black correction (0% reflectance) was performed by acquiring a dark image with the lens cap on. Regarding the portable camera, the white reference provided by the manufacturer, Konica Minolta Company, was recorded together with the painted panels and the painting, using the *Simultaneous white reference* option to directly control image quality, thus ensuring proper light exposure and time settings.

Data processing (including extraction of the images from the hyperspectral cube at different wavelengths and the spectral features and the application of functions for image pre-processing and processing) was carried out using Evince® (Prediktera, Umeå, Sweden), a comprehensive software toolkit for hyperspectral imaging. This software facilitates the exploration of multivariate modelling techniques to obtain and visualise chemical information hidden in images. In particular, the following features were obtained:

- RGB images with correction for tristimulus values (red = 630, green = 532, blue = 465).
- Punctual and average spectra for each pigment present on the selected areas, excluding those with traces of underdrawings, the translucent layers, and areas with gaps or imperfections.
- Application of the *2D contour* function, selecting the most representative wavelength to image the underdrawings. The images were converted to black and white.
- Application of the *PCA model* function to obtain a PCA plot along with a false-colour image showing the distribution of different materials.

All reflectance spectra were processed and compared using Origin 2018 data analysis and graphing software.

Additionally, Specim IQ® Studio software was used for supplementary data processing of the portable hyperspectral camera using an automated classification method. A database was created from the spectra acquired on the reference panels to define an identification model for real-case studies with unknown pigments. The software automatically highlighted areas containing reference pigments, linking known pigments to specific colours. Indeed, this model allowed for immediate classification of the results within the pigment distribution.

2.3. X-Ray Fluorescence (XRF)

X-ray Fluorescence (XRF) [54,55] was performed using a RX38 X-ray generator produced by EIS S.L.® featuring a W anode, coupled with an Al filter (1 mm thick), and a Silicon Drift Detector (SDD) with an energy resolution of 140 eV at the Mn-Kα line. The equipment used is unable to detect or reliably assess elements with an atomic number lower than Z = 14 (silicon). The handheld device was mounted on a specifically designed tripod equipped with handles to allow precise backward and forward movements, guided by the intersection of two integrated lasers for a fixed measuring distance. Each measurement

was conducted at 33.4 kV and 80 µA with an acquisition time of 200 s. The spectra were processed using PyMCA (version 5.9).

2.4. Ultraviolet Luminescence Photography (UVL)

For UVL images [56], a Nikon D3X camera was used with an ISO of 400 and an exposition time of 20 s. Homogeneous illumination of the painted surface was achieved by placing four Wood lamps (UVGL 55 Handheld UV lamp of UVP, λ = 254 and 365 nm) at 230 V/50 Hz, positioned at ~1 m, with two lamps on each side.

2.5. Infrared Reflectography (IRR)

IRR images [57,58] were obtained using two 800 W Halogen SDI lamps and a Xenics® Xeva-XS 512 camera (Xenics, Belgium) with an InGaAs detector mounted on a 2D robotic structure by Optimind, positioned 32 cm from the painting and remotely controlled using custom LabView® software (2023 Q3). A total of 15 images were taken and then stitched together using the ImageJ software.

3. Results and Discussion

3.1. Painted Panels

For the A-series VNIR hyperspectral camera mounted on the motorised stage, white (99% reflectance) and dark (0% reflectance) corrections were applied as described in Section 2.2, and the colour balance was adjusted using the tristimulus values for the RGB images (Figure 4). The reflectance spectra were then extracted from each painted square of the reference panels and normalised to allow their comparison (Figure 4E). In this way, it was possible to create a first personal database of the most common artists' materials used on polychrome surfaces and to compare the spectra with those available in the literature to confirm the correct detection [59–63]. Indeed, in the visible and near-infrared regions, different pigments and dyes have specific electronic and vibrational features due to electronic transitions [64].

The main features of the spectra, shown in the Supplementary Material (Figures S1 and S2), are listed in Table 4.

Table 4. Spectral characteristics of the pigments analysed.

Pigment	Spectral Shape	Peak Positions (nm)	Shift (Linseed Oil) (nm)	Attenuation (Arabic Gum) (%)
Verdigris	Single peak between	532–582	From 550 to 532	4
Malachite	Single peak between	525–548	From 545 to 525	9
Carmine	S-shaped band	600–620	From 600 to 620	2
Ultramarine	Single peak and shoulder-like band	448–471, 783	From 468 to 448	5
Vermilion	Shoulder-like band	617	-	-
Azurite	Main single peak and small shoulder-like band	470, 740	-	-
Haematite	Shoulder-like band next to the main single peak	600, 743	-	-
Yellow ochre	Double peak	584, 752	-	-
Lead-tin yellow	S-shaped band	500	-	-
White lead	Shoulder-like band	600	-	-

It is noteworthy that the samples showed a significant shift for some pigments in relation to different binders, highlighting the importance of comparing the case studies with references of pigments in the same binder. Small shifts through lower wavelengths were observed for pigments mixed with linseed oil and a small attenuation of the reflectance values

for those added to animal glue, mainly due to the different refractive indices of the binders (Figure S2). Indeed, the intensity and position of the reflectance spectra are influenced by the intrinsic properties of the suspensions, such as the pigment size, binder/pigment ratio, and the optical properties of both binder and pigment [65]. In this case, considering that the same pigment from the same batch was applied with different binders in the same amounts and thicknesses, it was possible to relate this spectral peculiarity to the contribution of the binder.

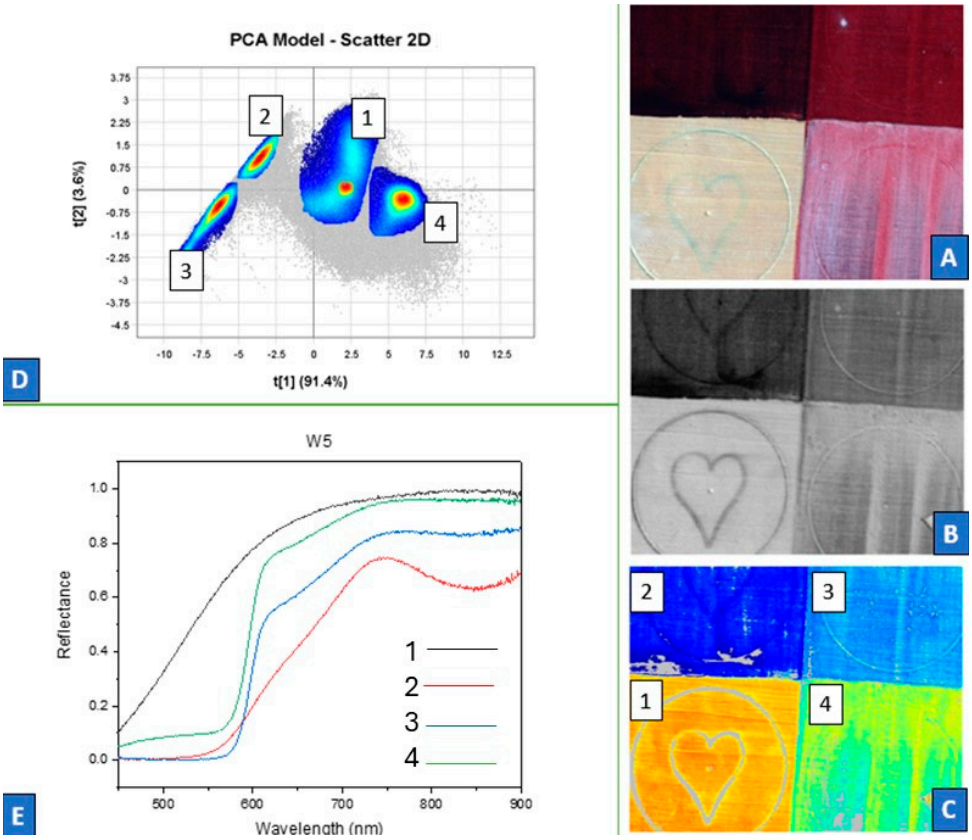

Figure 4. Data obtained from the VNIR hyperspectral camera mounted on the motorised stage: calibrated RGB image from panel W5 (**A**), image at 800 nm (**B**), false−colour image (**C**), PCA model graph (**D**), and spectra (**E**). The surface of the squares consists of white lead (1), haematite (2), vermilion (3), and lead−tin yellow (4). The false−colour image reflects their differentiation within four clusters of the PCA model graph (**D**). The image at 800 nm (**B**) shows the difficult detection through opaque pigments and multiple layers in the third and fourth areas. The spectra confirm the detection of lead-tin yellow (~500 nm) with the underneath layer of vermilion (617 nm) and haematite (743 nm).

Taking the tempera-based mixtures as a reference, verdigris, malachite, and ultramarine shifted by ~20 nm to lower wavelengths. Furthermore, carmine detection increased by 20 nm with linseed oil (Table 4). In addition, a general decrease in reflectance was observed for pigments mixed with arabic gum (Table 4). Regarding ultramarine blue, an inverse intensity was observed between the main single peak and the shoulder-like band. Thus, the higher reflectance (0.68) of the peak belonging to the linseed oil compound corresponds to the lower value of the shoulder-like band (0.62). On the other hand, for the mixture based on arabic gum, the lower value of the peak (0.3) is related to the higher intensity of the shoulder-like band (0.82). This shift, which depends on the binder, must be taken into account for correct pigment discrimination. Indeed, this aspect is particularly relevant when analysing unknown materials, considering the similarity of the spectra of some

pigments, as in the case of lead-tin yellow and white lead, carmine and vermilion, verdigris and malachite, and ultramarine and azurite.

In addition, the combination of several pigments in different layers made it possible to evaluate potential detection from underlying layers. Therefore, in the case of unknown multi-layer paintings, the lack of detection of a pigment under an optically opaque layer or the spectral contribution of a pigment from layers below the surface could be carefully considered. The main problem was the clear contribution of the haematite underlayer, identified in the spectra of the painted area with white lead, lead-tin yellow, azurite, and vermilion. The spectral features of haematite were easily identified in the pigments mentioned above, with the exception of vermilion. Indeed, the latter is difficult to identify in the presence of haematite, as the shoulder-like band at 617 nm can easily be confused with the one at 600 nm. In this case, a bump emerging in the spectral profile at 743 nm must be considered as a signal for the presence of haematite with vermilion.

The application of the PCA model function allowed the differentiation of all the pigments despite their similarity in colour or spectrum, thus proving to be an essential tool in the analysis of unknown materials. Indeed, this tool was used to find areas of interest, showing the different distributions of the data in the PCA graph (Figure 4D) and colouring the corresponding features in the hyperspectral false-colour images (Figure 4C). In all cases, more concentrated areas appeared as clouds of points, revealing the exact presence of the different colours on the surface of the painted tablets. Furthermore, the acquisition of the false colour image in conjunction with the PCA allowed the identification and classification of the different painted areas. Indeed, all the pigments were separated despite the presence of underlayers, even in the case of comparable pigments such as malachite and azurite, both opaque and characterised by a similar chemical formula (based on copper), or white lead and lead-tin yellow, both highly reflective and mainly composed of lead. In addition, in the juxtaposition of similar colours, the distinction between haematite and vermilion was noted (Figure 4), as well as between malachite and verdigris.

Between the analysed range (406.62–996.46 nm) with the VNIR hyperspectral camera fixed on the motorised stage, the 2D contour function was studied to ensure the possible dependence of the identification of the underdrawings, both in relation to the pigments and to the presence of different superimposed layers. The images at 800 nm proved to be the most useful for the detection of the drawing under the painted layers, although it was not possible to find clearly the graphite drawings under the opaque colours (malachite, azurite, and sometimes haematite). Probably, this drawback depends not only on the opacity of the pigments absorbing the light but also on the thickness of several layers (Figure 4B). Indeed, the third and fourth dials in the clockwise direction, consisting of three and four painted layers respectively, were difficult to detect.

However, by extending the wavelength range using the SWIR hyperspectral camera, drawings were generally detected between 1300–1600 nm, thus penetrating deeper into the layers [1]. In particular, for the opaque pigments, which were problematic with the VNIR hyperspectral camera, a suggestion of the designed graphite sketch under the painted layers was achieved thanks to the increased penetration, allowing the preparatory drawings to be revealed.

Furthermore, SWIR images were sensitive not only to different pigments but also to the thickness of the layers and the surface characteristics. Indeed, a distinction was made between thicker (third and fourth squares clockwise) and thinner (first and second squares clockwise) areas throughout the false-colour images (Figure 5). In addition, brush strokes, their different directions of application, rough surfaces, and uneven layers were enhanced. Consequently, the detection of these features can be used in the future to monitor technical and conservative aspects (i.e., craquelure) of the surface. In terms of spectra, all the areas analysed showed the same spectral profile (Figure 5), with an important contribution from the vibrational transition of water from the hydroxyl group (1200 nm), together with the characteristic triplet of hydroxyl first overtones and additional water combination bands from gypsum (1448–1492–1523 nm), and with the carbonate group from white lead

(1445–1200 nm) and azurite [64–66]. In the latter case, since the carbonate group from white lead in the priming layer was detected in all layer combinations, it was not possible to separate the carbonate contribution in the case of the simultaneous presence of azurite and white lead.

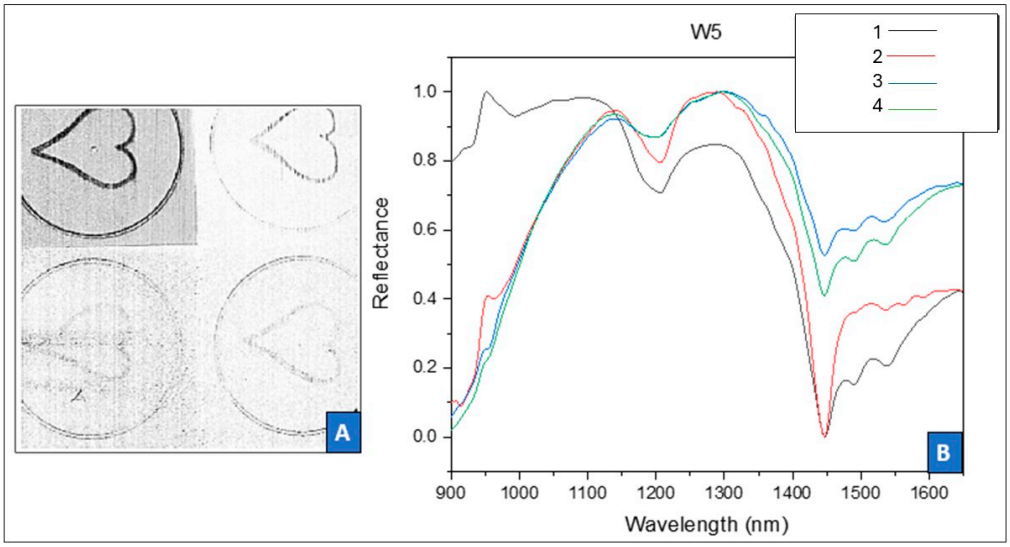

Figure 5. SWIR image of the W5 panel at 1400 nm (**A**) showing traces of the drawings from all squares and the spectral information coming from each area (**B**).

With regard to the portable VNIR hyperspectral camera (Specim IQ®), despite the higher noise of the data obtained with the A-series VNIR camera, it was possible to extract the same data with sufficient clarity both in terms of spectra identification and imaging processing, with the possibility of going deeper for the imaging of the drawings at 900 nm (Figure S3).

Furthermore, it was possible to define a model for the application of the classification method by uploading the reference spectra obtained from the analysis carried out on the panels. In particular, the different combinations of pigments on the panels made it possible to define a range of variance for each pigment to allow the system to automatically recognise the same pigment independently of the probable influences of the binder and the presence of different underlays. In addition, each reference pigment was assigned to a specific colour to be displayed in the areas containing that specific pigment. Thus, the software allowed obtaining different images showing the distribution of each identified pigment. Finally, all the images were stacked to obtain a complete figure showing the main distribution of the pigments detected.

3.2. First Application on the 17th-Century Oil Painting Virgen Con Niño

3.2.1. Ultraviolet Luminescence Photography (UVL) and Infrared Reflectography (IRR)

The UVL image (Figure 6a) allowed the identification of different retouches due to recent conservation interventions, which can be distinguished by the presence of bluish and brownish areas. In particular, the Virgin's complexion showed large areas of conservation, especially on the nose and forehead, with smaller dots distributed on the cheeks and the Child's legs and arms. Other significant areas of repainting were found on the Virgin's left hand and the Child's right arm. Another bright fluorescent area was identified in correspondence with the Virgin's hair, presumably related to the presence of varnish residues.

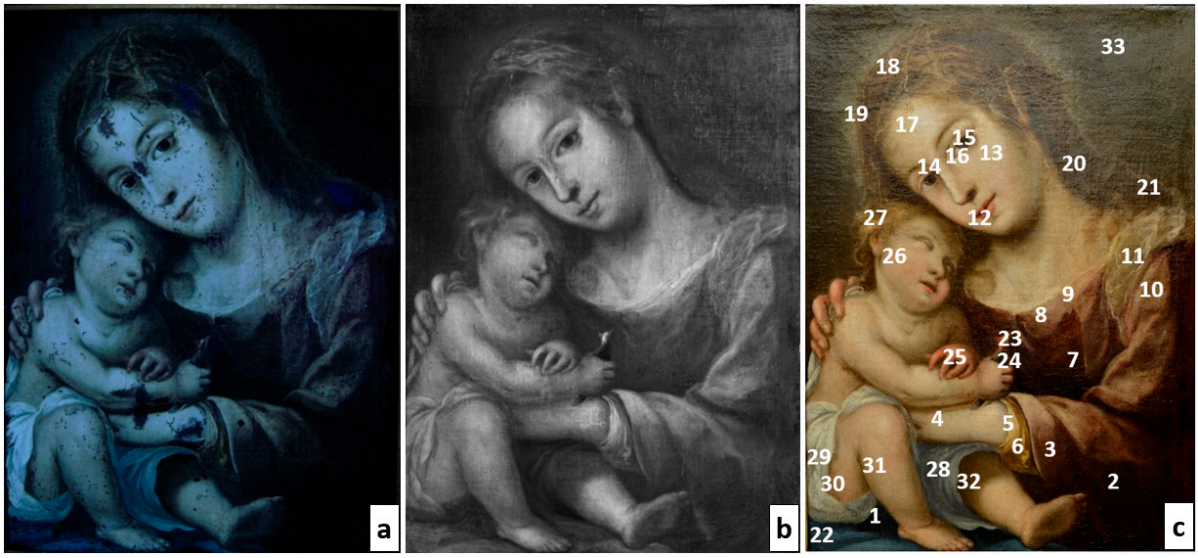

Figure 6. UVL (**a**), IRR (**b**), and points analysed using XRF (**c**).

In the IRR image (Figure 6b), restored areas were identified and confirmed in correspondence with the Child's nose, his arm, and partially in the Virgin's left wrist. The absence of the underdrawing suggests the painter did not carry out a preparatory drawing. This practice is attested in several 17th-century oil paintings when preparatory techniques were increasingly simplified. However, it is not possible to exclude less detailed sketches with poor detection contrast [67–70]. Furthermore, a dark area observed behind the Child's leg in the left corner may have been caused by a filling that was not fully visible under ultraviolet light.

The presence of retouched areas and the absence of a preparatory drawing provided useful information when interpreting the data for the first application of the hyperspectral cameras to test the efficiency of the parameters set on a real oil painting.

3.2.2. X-Ray Fluorescence (XRF)

X-ray fluorescence (XRF) was used to obtain the elemental characterisation of 33 points (Figure 6c) of different colours and tones to facilitate the correct recognition of the compounds when using the hyperspectral cameras. The results are presented in Table 5.

Table 5. Painted panels with applied pigments on different areas of the priming layer.

Point	Area	Elements	Pigments
1	Blue mantle	Ca ^{2}, Mn ^{1}, Pb ^{3}, Fe ^{2}	Prussian Blue, White Lead, Umber Earth
2	Reddish dress	Ca ^{2}, Fe ^{2}, Cu ^{1}, Hg ^{1}, Pb ^{3}	Vermilion, Red Ochre, Bone Black, Copper-Based Pigment
3	Light Brown Sleeve	Ca ^{2}, Fe ^{1}, Cu ^{1}, Pb ^{3}	Red Ochre, Bone Black, Copper-based pigment
4	Retouched area on the arm (yellowish)	Ca ^{2}, Ti ^{2}, Cr ^{1}, Mn ^{1}, Pb ^{3}, Hg ^{1}, Fe ^{1}, Zn ^{1}	Umber Earth, Chrome Yellow, Vermilion, Titanium White, Zinc White
5	Sleeve of the Virgin (light yellow)	Ca ^{2}, Fe ^{1}, Sn ^{2}, Pb ^{3}	Lead-Tin Yellow, Yellow Ochre, White Lead
6	Sleeve of the Virgin (dark yellow)	Ca ^{2}, Mn ^{1}, Fe ^{2}, Cu ^{1}, Sn ^{1}, Hg ^{1}, Pb ^{3}	Lead-Tin Yellow, Yellow Ochre, Umber Earth, Copper-based pigment
7	Dress	Ca ^{3}, Fe ^{1}, Cu ^{1}, Hg ^{1}, Pb ^{3}	Vermilion, Red Ochre, Copper-based pigment

Virgin

Table 5. *Cont.*

Point	Area	Elements	Pigments
8	Brownish collar	Ca [1], Pb [3], Hg [1], Cu [1], Fe [1]	Vermilion, Red Ochre, White Lead, Copper-based pigment
9	Light collar	Ca [2], Fe [1], Zn [1], Pb [3]	Zinc White, Ochre, White Lead
10	Brown sleeve	Ca [2], Fe [1], Cu [1], Pb [3]	Red Ochre, White lead, Copper-based pigment
11	Dark brown sleeve	Ca [2], Ti [1], Cr [1], Mn [1], Fe [2], Zn [1], Pb [3]	Titanium White, Zinc White, Yellow Ochre, Umber Earth, Manganese Black, White lead, Chromium Yellow
12	Lips	Ca [2], Fe [1], Hg [2], Pb [3]	Red Ochre, Vermilion, White Lead
13	Cheek	Ca [1], Fe [1], Sn [1], Hg [1], Pb [3]	Lead-Tin Yellow, Vermilion, White Lead, Red Ochre
14	Restored nostril	Ca [2], Ti [2], Cr [1], Fe [2], Zn [1], Hg [2], Pb [3]	Chromium Yellow, White Lead, Vermilion, Zinc White, White Lead, Red Ochre
15	Eye (brown)	Fe [2], Ca [2], Mn [1], Cu [1], Hg [1], Pb [3]	Umber Earth, Vermilion, Copper-based pigment
16	Eye (black)	Ca [3], Mn [1], Fe [2], Cu [1], Hg [1], Pb [3]	Manganese Black, Vermilion, Bone Black, Copper-based pigment
17	Restored forehead	Ca [2], Ti [3], Mn [1], Fe [2], Cr [1], Zn [3], Hg [1], Pb [3]	Chrome Yellow, Umber earth, White Lead, Zinc White, Titanium White
18	Hair (yellowish)	Ca [2], Mn [1], Fe [2], Cu [1], Hg [1], Pb [3]	Yellow Ochre, Umber Earth, Vermilion, Copper-based pigment
19	Hair (brown)	Ca [2], Mn [1], Fe [2], Cu [1], Hg [1], Pb [3]	Umber Earth, Yellow Ochre, Vermilion, Copper-based pigment
20		Ca [2], Mn [1], Fe [2], Zn [1], Cu [1], Hg [1], Pb [3]	Manganese Black, Red-Yellow Ochre, Vermilion, Zinc White, Copper-based pigment
21		Ca [3], Ti [1], Cr [1], Mn [1], Fe [2], Cu [1], Zn [1], Hg [1], Pb [3]	Titanium White, Zinc White, Manganese Black, Yellow Ochre, Vermilion, Chrome Yellow, White Lead, Copper-based pigment
22	Light Blue Dress	Pb [3], Ca [2], Fe [1]	White Lead, Prussian Blue
23	Goldfinch (Black)	Ca [2], Mn [1], Fe [2], Cu [1], Hg [2], Pb [3]	Manganese Black, Bone Black, Vermilion, Copper-based pigment
24	Goldfinch (Red)	Ca [2], Fe [1], Hg [3], Pb [3]	Vermilion, Red Ochre, White Lead
25	Cheek	Ca [2], Fe [1], Sn [1], Hg [1], Pb [3]	Lead-Tin Yellow, White Lead, Vermilion, Red Ochre
26	Reddish hand	Ca [2], Fe [1], Hg [2], Pb [3]	Vermilion, Red Ochre, White Lead
27	Hair	Ca [2], Mn [1], Fe [2], Cu [1], Hg [1], Pb [3]	Yellow Ochre, Manganese Black, Vermilion, White Lead, Copper-based pigment
28	Greyish mantle	Pb [3], Cu [1], Fe [2]	Prussian Blue, White lead, Azurite
29	White mantle	Ca [2], Fe [1], Pb [3]	White lead, Yellow Ochre
30	Dark skin tone of the leg	Ca [2], Fe [1], Hg [1], Pb [3]	Vermilion, White lead, Red Ochre
31	Light skin tone of the leg	Ca [1], Fe [1], Sn [1], Hg [2], Pb [3]	Vermilion, White lead, Red Ochre, Lead-Tin Yellow

Table 5. *Cont.*

Point		Area	Elements	Pigments
32	Child	Skin tone of the leg	Ca [2], Mn [1], Fe [2], Hg [1], Pb [3]	Vermilion, Manganese Black, Bone Black
33		Background (brown)	Ca [3], Ti [1], Fe [2], Mn [1], Zn [1], Pb [2]	Titanium White, Zinc White, Bone Black, Manganese Black, Ochre

[1]: main element; [2]: secondary element; [3]: minority element.

The distribution of calcium (Ca) and lead (Pb) found at all points indicates that the painting was probably prepared with gypsum ($CaSO_4 \cdot 2H_2O$) and/or calcium carbonate ($CaCO_3$), which were often applied as a base layer before the priming layer of rabbit glue and white lead ($(PbCO_3)2 \cdot Pb(OH)_2$). However, there is evidence that such materials were also commonly used as white pigments to lighten the colours of other pigments. Moreover, the presence of titanium (Ti) and zinc (Zn) highlighted the presence of pictorial retouches with titanium white (TiO_2) and zinc white (ZnO), applied later during various conservation treatments, particularly in the Virgin's forehead and nose, as previously identified in the UV images. Indeed, zinc white was synthesised and produced as a pigment at the end of the 18th century to replace the toxic lead white, while titanium white was a product of industrial development and commercially available since the 1920s [71].

These latter elements (Ti and Zn) were detected in the painting together with chromium (Cr) and lead (Pb) in brownish and yellowish areas, suggesting the use of different shades of chromium yellow ($PbCrO_4$), introduced as a pigment at the beginning of the 19th century [72]. Therefore, several conservative interventions took place in different periods (18th–20th century).

Concerning skin tones, mercury (Hg) and iron (Fe) indicate the use of cinnabar (HgS) and iron-based ochres (generally identified as asFe_2O_3 and α-FeOOH for the red and yellow typologies, respectively) [72]. Contemporary detection of lead (Pb) and tin (Sn) suggests the presence of lead-tin yellow (Pb2SnO4), known in antiquity as a glass opacifier, used in paintings from the 14th century but not extensively used until the second half of the 18th century [72]. However, taking into account that XRF is a semiquantitative analytical technique and the fluorescence yield and ionisation cross sections for lead and tin, the content of tin relative to lead does not match the stoichiometry of this yellow pigment, so it can be assumed that tin oxide can be found as an excess free agent, even if tin-containing cochineal lakes were produced in the 18th and 19th centuries [72]. The amount of these pigments has been shown to depend on the colour, so that the reddish areas are rich in vermilion and ochre, while the pale areas have consistently high levels of iron, probably related to ochre, together with white lead. Mercury (Hg) and iron (Fe) were also detected in the red areas, such as the Virgin's reddish dress and the goldfinch's red neck.

The brown areas are characterised by iron-based pigments, such as earth and natural ochres, mixed with black pigments to darken the shades. Among these, manganese (Mn) may be related to the use of umbra, which belongs to the group of earth pigments [72]. Furthermore, a considerable amount of calcium (Ca) cannot be exclusively associated with calcium carbonate from the preparatory layers, but it may also be related to the use of bone black and Vandyke brown [72]. Indeed, while the former is produced from partially charred bones, the latter was a humic earth brown, a hydrocarbon-based pigment with a low content of calcium carbonate, alumina, and silica, which was well-known in the palettes of 16th and 17th-century artists but difficult to detect by XRF due to its low sensitivity for low Z elements. In addition, although copper oxides are synthetic analogues of cuprite and tenorite with red and black colours, respectively, the source of the copper-based pigment (Cu) identified in the darkest areas cannot be specifically identified. Its presence seems to be linked to specific areas where no retouching has been detected, but historical copper pigments are green (verdigris, malachite, and copper resin) and blue (azurite), which could have been added to enhance the texture of these areas, which might otherwise have been flattened.

Concerning the main blue colour, the presence of iron (Fe) could be linked to the use of Prussian blue ($Fe_4[Fe(CN)_6]_3$), which was developed in the 18th century and is therefore an early addition, while the presence of copper (Cu) indicates the use of azurite [$Cu_3(CO_3)_2(OH)_2$].

3.2.3. Hyperspectral Imaging

The exploratory study on the oil painting was carried out by recording areas of interest to balance imaging sensitivity with data weight and sufficient detail for the imaged painting.

As shown in Figure 7, the false colour extraction did not seem to reflect separate groups of pigments, but rather different shades were assigned to areas where different pigments were used. However, the artistic technique of oil painting consists of the subsequent application of very thin layers of oil pigments, called veils, to modulate different shades, starting from dark tones and ending with highlights using light and white pigments. Therefore, the generation of the PCA graph reflects neighbouring clusters due to the presence of different mixtures. The selection of the data accumulation in the different groups indicated several areas based on the same features, from which it was possible to extract the spectral information. In addition, for each area, it was possible to apply the PCA model function to obtain the separation of different data of similar shades. However, it should be noted that the spectra were affected by higher noise than those extracted from the reference samples. Furthermore, it was possible to correctly identify most of the pigments previously found by XRF, according to the spectral features obtained in Section 3.1 *Painted* Panels and the characteristic spectral profile described in Table 3. Indeed, the skin tones resulted in a pigment based on haematite and yellow ochre (Figure 7D), in contrast to XRF, where only iron could be identified as the key element, thus not allowing a clear identification of red and yellow ochres. In addition, Cinnabar was detected in the reddish areas, as in the goldfinch. The same colours were confirmed in the dress of the Virgin, in different mixtures to obtain different shades. The presence of white lead and lead-tin-yellow in the light areas was confirmed.

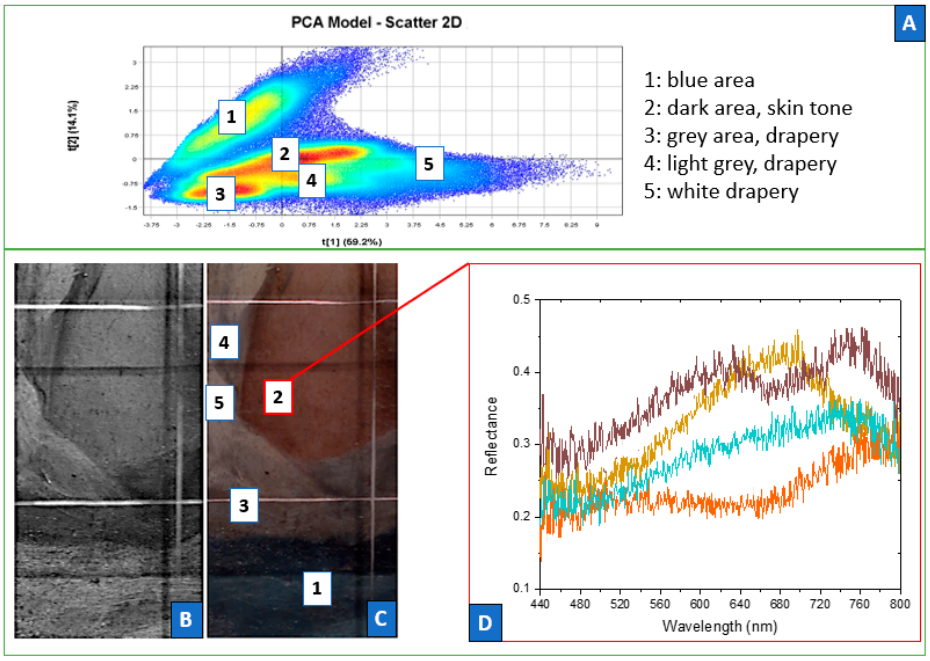

Figure 7. Selection of the Child's leg showing the PCA graph (**A**) with different clusters related to five different colour combinations corresponding to the labelled areas in the RGB image (**C**), the extraction of the image at 800 nm (**B**) with the enhancement of different surface characteristics, and

the extraction of the spectral information (**D**) from the skin tone, based on ochre and haematite in several mixtures with white lead and lead-tin yellow.

Azurite was detected in the blue parts with the characteristic peak and shoulder at 470 nm and 740 nm, respectively. Traces of azurite were also found in the sleeve, probably due to the copper-based pigment identified by XRF. Finally, in the retouched areas, a peak at the beginning (~410 nm) of the analysed region was identified as the contribution of titanium white [59,73] (Figure S4b).

About the 2D contour function, the image at 800 nm was extracted according to the preliminary analysis performed on the reference samples, thus enhancing the surface characteristics of the painting (Figure 7B). The absence of any underdrawing was demonstrated using the SWIR hyperspectral camera, which showed the noisy presence of the restored areas identified in the infrared reflectography, together with the enhancement of the brushes, texture, and *craquelure* that affected the surface (Figure S4).

The use of the portable VNIR hyperspectral camera allowed the direct detection of the main pigments, selecting the areas of interest on the touch screen simultaneously with the image acquisition, thanks to the reference spectra established after the analyses carried out on the panels. As in the case of the reference painted panels, the data acquisition on the oil painting was compared with that previously described for the VNIR camera mounted on the motorised stage, despite the higher noise. Indeed, the application of the 2D contour function made it possible to obtain better details of the surface condition, while the plotted PCA model made it possible to group the data in terms of the different spectral information contained in the associated false colour images. A further improvement was obtained by applying the classification method previously configured in the reference plates (Figure 8). It was possible to extract different images illustrating the distribution of the main related pigments, which were finally combined in a single image that generally reflected the main pigments used by the painter (Figure 8).

Figure 8. Application of the classification method for the handheld VNIR hyperspectral camera using

Specim IQ® software: test for fast in situ analyses run after the creation of the library (**A**), stacked images of the distribution of the main pigments (**B**), and a series of images showing the distribution of the pigments in a selected area (**C**).

Therefore, a summary comparison of the advantages and disadvantages of the three different hyperspectral cameras has been listed in Table 6, together with the level of success of feature detection by the explored imaging tools (2D contour function, PCA model, and PCA false colour image). The symbols ✔ and X represent the positive and negative applications of the different cameras in pigment identification, respectively. In this way, conservators can be aware of the potential issues when using hyperspectral cameras, being able to make informed considerations regarding the analytical conditions and the data interpretation. Moreover, the protocol can be implemented as required for any typology of painting, creating new panels with pigments of interest applied within several binders. Therefore, it will be possible to enlarge the spectral databases within specific painting applications, enabling conservators to boost the routine use of hyperspectral cameras across multiple case studies.

Table 6. Information gained using the three different hyperspectral cameras.

Oil Painting			Panels			Test	
Motorized SWIR	**Motorized VNIR**	**Portable VNIR**	**Motorized SWIR**	**Motorized VNIR**	**Portable VNIR**	**Camera**	
X	✔		X	✔	✔	Spectra of the pigments	Applications
Imaging of brushstrokes, craquelure, conservation state			1. Drawing at ~1300–1400 nm 2. Very good im-age of brushstrokes, craquelure, sur-face conservation	1. Drawing at ~800 nm but losing information on very opaque and multilayered areas 2. Good imaging of brushstroke, craquelure, and sur-face conservation state		Wavelength selection (2D contour function)	
False separation due to IR information related to the vibrational bonds	Small separation (due to the abundance of mixtures from the oil technique)		False separation due to IR information related to the vibrational bonds	Very good separation	Good separation	PCA model	
Enhancement of the surface and brushes	Better differentiation on small selections		Enhancement of the surface, conservation state and brushstrokes	Very good visual differentiation even in similar colours	Good visual differentiation even in similar colours	PCA false colour image	
High penetration in depth	High image and spectra resolution, very good RGB image	1. Portable, quick calibration, large area/whole painting 2. Classification method	High penetration in depth	High image and spectra resolution, very good RGB images	Portable, quick calibration, large areas/whole painting	Advantages	
Small areas of analysis, rough surface	Small areas of analysis	Low resolution, noisy spectra	Small areas of analysis		Low resolution and noisy spectra	Disadvantages	

4. Conclusions

The collaboration between the Centro Nacional de Aceleradores (CNA) and the Laboratory of Applied Physics (GFI) of the School of Engineering (ETSI) of the University of Seville has allowed the application of three different hyperspectral (HSI) cameras to

this study of ancient paintings. In particular, after testing painted reference panels, it was possible to evaluate the best working conditions of the cameras for future non-invasive and non-destructive characterisations of the vast collection of paintings from the Archbishop's Palace and the Cathedral of Seville.

Indeed, the exploration of data handling and processing using the Evince® software revealed the possibility of easily obtaining quick information from the hyperspectral cube using the PCA modelling functions and the associated spectral extraction. As a result, the Conservation Laboratory will take advantage of simple surveys on polychrome surfaces, starting from the spatial and spectral information within the quick classification method set on the handheld VNIR hyperspectral camera as a first screening test, followed by the use of VNIR and SWIR hyperspectral cameras mounted on motorised stages. Complementary information is then obtained by applying different methods, such as X-ray fluorescence (XRF) analysis, to specific points of interest highlighted in the first step of the investigation by multispectral and hyperspectral imaging methods.

Finally, this study has opened up new perspectives for the application of hyperspectral cameras in the field of cultural heritage, so that it will be possible to extend the database of reference materials for oil paintings, including contemporary materials for the detection of late retouches and restorations. Moreover, new tests will be elaborated with the development of different algorithms for multivariate analysis and deep learning network models with simplified procedures for conservators.

Supplementary Materials: The following supporting information can be downloaded at: https://www.mdpi.com/article/10.3390/heritage7110281/s1, Figure S1: Examples of the spectra obtained with the VNIR hyperspectral camera; Figure S2: Influence of the binder; Figure S3: Representative collage showing the data obtained from the handheld VNIR hyperspectral: the calibrated RGB image from panel W5 in the inset of the PCA graph (a), the false colour image (b), the extracted image at 900 nm (c), and the spectra from each square of the panel (d). Despite noisy information and similar colour assigned to the red pigments, the false colour image reflects the differentiation between lead white (1), hematite (2), vermilion (3) and lead-tin yellow (4) respectively found in the clusters of the PCA model graph. Regarding the drawings, the image at 900 nm (c) shows traces of the drawing under the third square and the lack of detection under the fourth area. Finally, the spectra (d) confirm the mixture between lead-tin yellow with the underneath layer of vermilion with the mixed information coming from the bump at ~500 nm for lead-tin yellow and the characteristic fingerprint of vermilion at 617 nm and the emerging peak of hematite at 743 nm; Figure S4: Retouched areas identified when using the hyperspectral cameras: SWIR image showing enhanced roughness of the surface and the presence of retouches on the nose of the Virgin highlighted by the red arrow (a) and traces from titanium white identified at ~410 nm (b) among the spectra extracted from the black selection on the nose of the Virgin shown in the false colour image (e), the image obtained at 800 nm (d) and the PCA graph (c)

Author Contributions: G.V.: Conceptualisation; Data curation; Formal analysis; Investigation; Methodology; Validation; Visualization; Writing—original draft; Writing—review and editing. H.A.: Data curation; Formal analysis; Investigation; Methodology; Validation; Visualization; Writing—review and editing. I.F.-L.: Conceptualization; Formal analysis; Methodology; Writing—review and editing; J.M.-S.: Formal analysis; Investigation; Writing—review and editing; A.K.: Formal analysis; Methodology; R.P.-G.: Conceptualization; Formal analysis; Methodology; E.G.-G.: Conceptualisation; Methodology; Validation; Project administration; Resources; Software; Supervision; M.A.R.G.: Conceptualisation; Methodology; Validation; Project administration; Supervision. All authors have read and agreed to the published version of the manuscript.

Funding: This research did not receive any specific grant from funding agencies in the public, commercial, or not-for-profit sectors. The cameras and equipment used in this research were funded by Grant Numbers COV20-00080 and COV20-00173 of the 2020 Emergency Call for Research Projects about the SARS-CoV-2 virus and the COVID-19 disease of the Institute of Health 'Carlos III', Spanish Ministry of Science and Innovation, and by Grant Number EQC2019-006240-P funded by MICIN/AEI/10.13039/501100011033 and by "ERDF: A Way of Making Europe". ABR was

supported by Grant Number RTI2018-094465-J-I00 funded by MICIN/AEI/10.13039/501100011033 and by "ERDF: A Way of Making Europe".

Data Availability Statement: The data supporting the findings of this study are available from the corresponding author, G.V., upon reasonable request.

Acknowledgments: The authors thank the conservators Augustín Martín de Soto and Antonio Gamero Osuna from the Conservation Laboratory of the Archbishop's Palace and the priest Don Antonio for their valuable collaboration and their constant efforts for the preservation of the precious cultural heritage of the Cathedral and the Curia of Seville. Moreover, the authors dedicate this study to the beloved professor Emilio Gomez Gonzalez, who prematurely died before the submission of this paper. The academic world has dramatically lost an immense professor, a tireless worker, and a generous person. It was an honour for the authors to work with such a marvellous colleague and friend.

Conflicts of Interest: The authors declare no conflict of interest.

References

1. George, S.; Hardeberg, J.Y.; Linhares, J.; MacDonald, L.; Montagner, C.; Nascimento, S.; Picollo, M.; Pillay, R.; Vitorino, T.; Keats Webb, E. A Study of Spectral Imaging Acquisition and Processing For Cultural Heritage. In *Digital Techniques for Documenting and Preserving Cultural Heritage*; Arc Humanities Press: Yorkshire, UK, 2018; pp. 141–158.
2. Shukla, A.; Kot, R. An Overview of Hyperspectral Remote Sensing and its applications in various Disciplines. *IRA-Int. J. Appl. Sci.* **2016**, *5*, 85. [CrossRef]
3. Kubik, M. Chapter 5 Hyperspectral Imaging: A New Technique for the Non-Invasive Study of Artworks. *Phys. Tech. Study Art Archaeol. Cult. Herit* **2007**, *2*, 199–259.
4. MacDonald, L.W.; Vitorino, T.; Picollo, M.; Pillay, R.; Obarzanowski, M.; Sobczyk, J.; Nascimento, S.; Linhares, J. Assessment of multispectral and hyperspectral imaging systems for digitisation of a Russian icon Enhanced Reader. *Herit. Sci.* **2017**, *5*, 1–6. [CrossRef]
5. Li, G.H.; Chen, Y.; Sun, X.J.; Duan, P.Q.; Lei, Y.; Zhang, L.F. An automatic hyperspectral scanning system for the technical investigations of Chinese scroll paintings Enhanced Reader. *Microchem. J.* **2020**, *155*, 104699. [CrossRef]
6. Cucci, C.; Casini, A.; Stefani, L.; Picollo, M.; Jussila, J. Bridging research with innovative products: A compact hyperspectral camera for investigating artworks: A feasibility study. In *Optics for Arts, Architecture, and Archaeology VI*; SPIE: Île-de-France, France, 2017; p. 1033106.
7. Mounier, A.; Le Bourdon, G.; Aupetit, C.; Belin, C.; Servant, L.; Lazare, S.; Lefrais, Y.; Daniel, F. Hyperspectral imaging, spectrofluorimetry, FORS and XRF for the non-invasive study of medieval miniatures materials. *Herit. Sci.* **2014**, *2*, 24. [CrossRef]
8. Gomez-Gonzalez, E.; Barriga-Rivera, A.; Fernandez-Muñoz, B.; Navas-Garcia, J.M.; Fernandez-Lizaranzu, I.; Munoz-Gonzalez, F.J.; Parrilla-Giraldez, R.; Requena-Lancharro, D.; Gil-Gamboa, P.; Rosell-Valle, C.; et al. Optical imaging spectroscopy for rapid, primary screening of SARS-CoV-2: A proof of concept. *Sci. Rep.* **2022**, *12*, 2356. [CrossRef]
9. Amigo, J.M.; Babamoradi, H.; Elcoroaristizabal, S. Hyperspectral image analysis. *A Tutorial. Anal. Chim. Acta.* **2015**, *896*, 34–51. [CrossRef]
10. Thomas, S.; Kuska, M.T.; Bohnenkamp, D.; Brugger, A.; Alisaac, E.; Wahabzada, M.; Behmann, J.; Mahlein, A.K. Benefits of hyperspectral imaging for plant disease detection and plant protection: A technical perspective. *J. Plant Dis. Prot.* **2018**, *125*, 5–20. [CrossRef]
11. Cheng, J.-H.; Sun, D.-W. Recent Applications of Spectroscopic and Hyperspectral Imaging Techniques with Chemometric Analysis for Rapid Inspection of Microbial Spoilage in Muscle Foods. *Compr. Rev. Food Sci. Food Saf.* **2015**, *14*, 478–490. [CrossRef]
12. Terra, L.R.; Roque, J.V.; Pola, C.C.; Gonçalves, I.M.; Soares, N.d.F.F.; Teófilo, R.F. Study of chemical compound spatial distribution in biodegradable active films using NIR hyperspectral imaging and multivariate curve resolution. *J. Chemom.* **2020**, *34*, e3193. [CrossRef]
13. Hossain, A. Spectral simulation and method design of camouflage textiles for concealment of hyperspectral imaging in UV-Vis-IR against multidimensional combat background. *J. Text. Inst.* **2023**, *114*, 331–342. [CrossRef]
14. Tahmasbian, I.; Morgan, N.K.; Hosseini Bai, S.; Dunlop, M.W.; Moss, A.F. Comparison of Hyperspectral Imaging and Near-Infrared Spectroscopy to Determine Nitrogen and Carbon Concentrations in Wheat. *Remote Sens.* **2021**, *13*, 1128. [CrossRef]
15. Priyashantha, H.; Höjer, A.; Saedén, K.H.; Lundh, Å.; Johansson, M.; Bernes, G.; Geladi, P.; Hetta, M. Use of near-infrared hyperspectral (NIR-HS) imaging to visualize and model the maturity of long-ripening hard cheeses. *J. Food Eng.* **2020**, *264*, 109687. [CrossRef]
16. Cosentino, A. Multispectral imaging system using 12 interference filters for mapping pigments. *Conserv. Patrim.* **2015**, *21*, 25–38. [CrossRef]
17. Cucci, C.; Casini, A. Hyperspectral imaging for artworks investigation. In *Data Handling in Science and Technology*; Elsevier Ltd.: Amsterdam, The Netherlands, 2020; pp. 583–604.

18. Amigo, J.M.; Grassi, S. Configuration of hyperspectral and multispectral imaging systems. In *Data Handling in Science and Technology*; Elsevier Ltd.: Amsterdam, The Netherlands, 2019; pp. 17–34.
19. Qureshi, R.; Uzair, M.; Khurshid, K.; Yan, H. Hyperspectral document image processing: Applications, challenges and future prospects. *Pattern Recognit.* **2019**, *90*, 12–22. [CrossRef]
20. Pillay, R.; Hardeberg, J.Y.; George, S. Hyperspectral imaging of art: Acquisition and calibration workflows. *J. Am. Inst. Conserv.* **2019**, *58*, 3–15. [CrossRef]
21. Gillooly, T.; Deborah, H.; Hardeberg, J.Y. Path Opening for Hyperspectral Crack Detection of Cultural Heritage Paintings. In Proceedings of the 14th International Conference on Signal Image Technology and Internet Based Systems, SITIS 2018, Las Palmas de Gran Canaria, Spain, 26–29 November 2018; Institute of Electrical and Electronics Engineers Inc.: Piscataway, NJ, USA, 2018; pp. 651–657.
22. Liang, H. Advances in multispectral and hyperspectral imaging for archaeology and art conservation. *Appl. Phys. A* **2012**, *106*, 309–323. [CrossRef]
23. Fischer, C.; Kakoulli, I. Multispectral and hyperspectral imaging technologies in conservation: Current research and potential applications. *Stud. Conserv.* **2006**, *51*, 3–16. [CrossRef]
24. Bayarri, V.; Sebastián, M.A.; Ripoll, S. Hyperspectral Imaging Techniques for the Study, Conservation and Management of Rock Art. *Appl. Sci.* **2019**, *9*, 5011. [CrossRef]
25. Rohani, N.; Pouyet, E.; Walton, M.; Cossairt, O.; Katsaggelos, A.K. Nonlinear Unmixing of Hyperspectral Datasets for the Study of Painted Works of Art. *Angew. Chem. Int. Ed.* **2018**, *57*, 10910–10914. [CrossRef]
26. Cucci, C.; Webb, E.K.; Casini, A.; Ginanni, M.; Prandi, E.; Stefani, L.; Vitorino, T.; Picollo, M. Short-wave infrared reflectance hyperspectral imaging for painting investigations: A methodological study. *J. Am. Inst. Conserv.* **2019**, *58*, 16–36. [CrossRef]
27. Sandak, J.; Sandak, A.; Legan, L.; Retko, K.; Kavčič, M.; Kosel, J.; Poohphajai, F.; Diaz, R.H.; Ponnuchamy, V.; Sajinčič, N.; et al. Nondestructive Evaluation of Heritage Object Coatings with Four Hyperspectral Imaging Systems Enhanced Reader. *Coatings* **2021**, *11*, 244. [CrossRef]
28. Kolokoussis, P.; Skamantzari, M.; Tapinaki, S.; Karathanassi, V.; Georgopoulos, A. 3D and Hyperspectral Data Integration for Assessing Material Degradation in Medieval Masonry Heritage Buildings. *Int. Arch. Photogramm. Remote Sens. Spat. Inf. Sci.* **2021**, *XLIII-B2-2021*, 583–590. [CrossRef]
29. Delaney, J.K.; Picollo, M. JAIC special issue on "Reflectance hyperspectral imaging to support documentation and conservation of 2D artworks". *J. Am. Inst. Conserv.* **2019**, *58*, 1–2. [CrossRef]
30. Delaney, J.K.; Zeibel, J.G.; Thoury, M.; Littleton, R.; Palmer, M.; Morales, K.M.; de la Rie, R.; Hoenigswald, A. Visible and Infrared Imaging Spectroscopy of Picasso's *Harlequin Musician*: Mapping and Identification of Artist Materials in Situ. *Appl. Spectrosc.* **2010**, *64*, 584–594. [CrossRef]
31. Sciuto, C.; Cantini, F.; Chapoulie, R.; Cou, C.; De la Codre, H.; Gattiglia, G.; Granier, X.; Mounier, A.; Palleschi, V.; Sorrentino, G.; et al. What Lies Beyond Sight? Applications of Ultraportable Hyperspectral Imaging (VIS-NIR) for Archaeological Fieldwork. *J. Field Archaeol.* **2022**, *47*, 522–535.
32. Babini, A.; Lombardo, T.; Schmidt-Ott, K.; George, S.; Hardeberg, J.Y. Acquisition strategies for in-situ hyperspectral imaging of stained-glass windows: Case studies from the Swiss National Museum. *Herit. Sci.* **2023**, *11*, 74. [CrossRef]
33. Daveri, A.; Paziani, S.; Marmion, M.; Harju, H.; Vidman, A.; Azzarelli, M.; Vagnini, M. New perspectives in the non-invasive, in situ identification of painting materials: The advanced MWIR hyperspectral imaging. *TrAC Trends Anal. Chem.* **2018**, *98*, 143–148. [CrossRef]
34. Padoan, R.; Steemers, T.; Klein, M.; Aalderink, B. Quantitative Hyperspectral Imaging of Historical Documents: Technique and Application. In Proceedings of the 9th International Conference ART Proc., Jerusalem, Israel, 25–30 May 2008; pp. 25–30.
35. Snijders, L.; Zaman, T.; Howell, D. Using hyperspectral imaging to reveal a hidden precolonial Mesoamerican codex. *J. Archaeol. Sci. Rep.* **2016**, *9*, 143–149. [CrossRef]
36. Bayliss, S.; van den Berg, K.J.; Burnstock, A.; de Groot, S.; van Keulen, H.; Sawicka, A. An investigation into the separation and migration of oil in paintings by Erik Oldenhof. *Microchem. J.* **2016**, *124*, 974–982. [CrossRef]
37. Erhardt, D.; Tumosa, C.S.; Mecklenburg, M.F. Long-Term Chemical and Physical Processes in Oil Paint Films. *Stud. Conserv.* **2005**, *50*, 143–150. [CrossRef]
38. Izzo, F.C.; van den Berg, K.J.; van Keulen, H.; Ferriani, B.; Zendri, E. *Modern Oil Paints—Formulations, Organic Additives and Degradation: Some Case Studies*; Issues in Contemporary Oil Paint; Springer International Publishing: Cham, Switzerland, 2014; pp. 75–104.
39. Frey, F.; Heller, D.; Kushel, D.; Vitale, T.; Weaver, G. *The AIC Guide to Digital Photography and Conservation Documentation*, 2008th ed.; Warda, J., Ed.; American Institute for Conservation of Historic and Artistic Works: Washington, DC, USA, 2008.
40. Thomson Cbe, G. *Museum Environment*; Routledge: Informa, UK, 2018.
41. Clementi, C.; Miliani, C.; Verri, G.; Sotiropoulou, S.; Romani, A.; Brunetti, B.G.; Sgamellotti, A. Application of the Kubelka—Munk Correction for Self-Absorption of Fluorescence Emission in Carmine Lake Paint Layers. *Appl. Spectrosc.* **2009**, *63*, 1323–1330. [CrossRef]
42. Dupuis, G.; Menu, M. Quantitative characterisation of pigment mixtures used in art by fibre-optics diffuse-reflectance spectroscopy. *Appl. Phys. A* **2006**, *83*, 469–474. [CrossRef]

43. Gomes Gonçalves, Í.; Petter, C.O.; Lepkoski Machado, J. Quantification of Hematite and Goethite Concentrations in Kaolin Using Diffuse Reflectance Spectroscopy: A New Approach To Kubelka-Munk Theory. *Clays Clay Miner.* **2012**, *60*, 473–483. [CrossRef]
44. Latour, G.; Elias, M.; Frigerio, J.-M. Determination of the Absorption and Scattering Coefficients of Pigments: Application to the Identification of the Components of Pigment Mixtures. *Appl. Spectrosc.* **2009**, *63*, 604–610. [CrossRef]
45. Pozo-Antonio, J.S.; Cardell, C.; Sánchez, S.; Montes Rueda, J. Reflectance of Oil Paintings: Influence of Paint Layer Thickness and Binder Amount. *Coatings* **2022**, *12*, 601. [CrossRef]
46. Cucci, C.; Casini, A.; Picollo, M.; Poggesi, M.; Stefani, L. Open issues in hyperspectral imaging for diagnostics on paintings: When high-spectral and spatial resolution turns into data redundancy. *O3A Opt. Arts Archit. Archaeol. III* **2011**, *8084*, 4131–4140.
47. Datta, A.; Ghosh, S.; Ghosh, A. PCA, Kernel PCA and Dimensionality Reduction in Hyperspectral Images. In *Advances in Principal Component Analysis*; Springer Singapore: Singapore, 2018; pp. 19–46.
48. Imani, M.; Ghassemian, H. Principal component discriminant analysis for feature extraction and classification of hyperspectral images. In Proceedings of the 2014 Iranian Conference on Intelligent Systems (ICIS), Bam, Iran, 4–6 February 2014; pp. 1–5.
49. Deepa, P.; Thilagavathi, K. Feature extraction of hyperspectral image using principal component analysis and folded-principal component analysis. In Proceedings of the 2015 2nd International Conference on Electronics and Communication Systems (ICECS), Coimbatore, India, 26–27 February 2015; pp. 656–660.
50. Imani, M.; Ghassemian, H. An overview on spectral and spatial information fusion for hyperspectral image classification: Current trends and challenges. *Inf. Fusion* **2020**, *59*, 59–83. [CrossRef]
51. Pouyet, E.; Miteva, T.; Rohani, N.; de Viguerie, L. Artificial Intelligence for Pigment Classification Task in the Short-Wave Infrared Range. *Sensors* **2021**, *21*, 6150. [CrossRef]
52. Radpour, R. *An Alternative Approach to Mapping Pigments in Paintings with Hyperspectral Reflectance Image Cubes Using Artificial Intelligence Enhanced Reader*; University of California: Los Angeles, CA, USA, 2019.
53. Gomez-Gonzalez, E.; Fernandez-Muñoz, B.; Barriga-Rivera, A.; Navas-Garcia, J.M.; Fernandez-Lizaranzu, I.; Munoz-Gonzalez, F.J.; Parrilla-Giraldez, R.; Requena-Lancharro, D.; Guerrero-Claro, M.; Gil-Gamboa, P.; et al. Hyperspectral image processing for the identification and quantification of lentiviral particles in fluid samples. *Sci. Rep.* **2021**, *11*, 16201. [CrossRef]
54. Janssens, K. *Chapter 4 X-ray Based Methods of Analysis*; Elsevier: Amsterdam, The Netherlands, 2004; pp. 129–226.
55. Ferretti, M. X-ray Fluorescence Applications for the Study and Conservation of Cultural Heritage. In *Radiation in Art and Archeometry*; Elsevier: Amsterdam, The Netherlands, 2000; pp. 285–296.
56. Mairinger, F. The ultraviolet and fluorescence study of paintings and manuscripts. In *Radiation in Art and Archeometry*; Elsevier: Amsterdam, The Netherlands, 2000; pp. 56–75.
57. Mairinger, F. The infrared examination of paintings. In *Radiation in Art and Archeometry*; Elsevier: Amsterdam, The Netherlands, 2000; pp. 40–55.
58. Van Asperen de Boer, J.R.J. Infrared Reflectography: A Method for the Examination of Paintings. *Appl. Opt.* **1968**, *7*, 1711. [CrossRef]
59. Cosentino, A. FORS Spectral Database of Historical Pigments in Different Binders. *E-Conserv. J.* **2014**, *2*, 54–65. [CrossRef]
60. Torrent, J.; Barrón, V. (Eds.) Diffuse Reflectance Spectroscopy. In *Diffuse Reflectance Spectroscopy of Iron Oxides*; University of Cordoba: Córdoba, Spain, 2008.
61. Dupuis, G.; Elias, M.; Simonot, L. Pigment Identification by Fiber-Optics Diffuse Reflectance Spectroscopy. *Appl. Spectrosc.* **2002**, *56*, 1329–1336. [CrossRef]
62. Ferrer, D.H.J.S.; Sandu, I.C.; George, S.; Hardeberg, J.Y. Old Man in Warnemünde (1907) Colouring Palette: A Case Study on the Use of Hyperspectral Imaging for Pigment Identification. In *Color and Imaging Conference*; Society for Imaging Science and Technology: Lillehammer, Norway, 2017; pp. 339–344.
63. Kartsonak, M.; Koui, M.; Callet, P.; Cheilakou, E. Non-destructive identification of the coloring substances of the monuments studied using colorimetry. In Proceedings of the 4th International Conference on NDT, Crete, Greece, 11–14 October 2007.
64. Cucci, C.; Delaney, J.K.; Picollo, M. Reflectance Hyperspectral Imaging for Investigation of Works of Art: Old Master Paintings and Illuminated Manuscripts. *Acc. Chem. Res.* **2016**, *49*, 2070–2079. [CrossRef]
65. Derrick, M.R.; Stulik, D.C.; Landry, J.M. *Infrared Spectroscopy in Conservation Science*; The Getty Institute: Los Angeles, CA, USA, 1999.
66. Murphy, R.; Chlingaryan, A.; Melkumyan, A. Predicting Wavelength Position of the Ferric Iron Absorption at −900 nm from Hyperspectral Data (1000–2500 nm). In Proceedings of the 36th APCOM Applications of Computers and Operations Research in the Mineral Industry, Porto Alegre, Brazil, 4–8 November 2013.
67. Lefèvre, W. *Inside the Camera Obscura—Optics and Art under the Spell of the Projected Image*; Max Planck Institute for the History of Science: Berlin, Germany, 2007.
68. Le Chanu, P. *Contributions and Limitations of Scientific Examination and Analysis in the Detection of Forgeries of Old Masters' Paintings*; McCrone, W., Chartier, D.R., Weiss, R.J., Eds.; SPIE: San Jose, CA, USA, 1998; pp. 62–73.
69. Antunes, V.; Valadas, S.; Serrão, V.; Carvalho, M.L.; Candeias, A.; Mirão, J.; Cardoso, A.; Pessanha, S.; Manso, M. Josefa d' Óbidos workshop from panel to canvas. Multianalytical approach to materials and technical evolution of the most significant Portuguese painting workshop of the 17th century. *J. Mol. Struct.* **2019**, *1188*, 31–41. [CrossRef]
70. Locquet, A.; Dong, J.; Citrin, D.S.; Melis, M. Terahertz pulsed imaging reveals the stratigraphy of a seventeenth-century oil painting. In *Unconventional Optical Imaging*; Fournier, C., Georges, M.P., Popescu, G., Eds.; SPIE: Île-de-France, France, 2018; p. 71.

71. West Fitzhugh, E. *Artists' Pigments: A Handbook of Their History and Characteristic*; National Gallery of Art: Washington, DC, USA, 2012.
72. Eastaugh, N.; Walsh, V.; Chaplin, T.; Siddall, R. *Pigment Compendium: A Dictionary and Optical Microscopy of Historical Pigments*; Routledge Series in Conservation and Museology; Routledge: London, UK, 2008.
73. Pronti, L.; Felici, A.C.; Ménager, M.; Vieillescazes, C.; Piacentini, M. Spectral Behavior of White Pigment Mixtures Using Reflectance, Ultraviolet—Fluorescence Spectroscopy, and Multispectral Imaging. *Appl. Spectrosc.* **2017**, *71*, 2616–2625. [CrossRef]